Ab initio investigation of impurity-induced in-gap states in Bi_2Te_3 and Bi_2Se_3

Juba Bouaziz,[1,*] Manuel dos Santos Dias,[1,†] Julen Ibañez-Azpiroz,[1,2] and Samir Lounis[1,‡]
[1]*Peter Grünberg Institut and Institute for Advanced Simulation, Forschungszentrum Jülich and JARA, 52425 Jülich, Germany*
[2]*Materials Physics Center, CSIC-UPV/EHU, 20018 Donostia-San Sebastián, Spain*

(Received 27 April 2018; published 16 July 2018)

We investigate in-gap states emerging when a single 3*d* transition metal impurity is embedded in topological insulators (Bi_2Te_3 and Bi_2Se_3). We use a combined approach relying on first-principles calculations and an Anderson impurity model. By computing the local density of states of Cr, Mn, Fe, and Co embedded not only in surfaces of Bi_2Te_3 and of Bi_2Se_3 but also in their bulk phases, we demonstrate that in-gap states originate from the hybridization of the electronic states of the impurity with bulk bands and not with the topological surface states as is usually assumed. This finding is analyzed using a simplified Anderson impurity model. These observations are in contradiction with the prevailing models used to investigate the magnetic doping of topological insulators [R. R. Biswas *et al.*, Phys. Rev. B **81**, 233405 (2010)], which attribute the origin of the in-gap states to the hybridization with the topological surface states.

DOI: 10.1103/PhysRevB.98.035119

I. INTRODUCTION

The concept of band topology was introduced in condensed matter physics in the context of the quantum Hall effect (QHE) [1,2], which represents a quantized version of the classical Hall effect [3]. The QHE is observed in two-dimensional electronic systems at low temperatures and under strong magnetic fields applied perpendicularly to the plane containing the electrons [1,2]. In the classical picture, the electrons can be viewed as charges moving in circles around a magnetic field. At the edges of the sample, the circles are not completed giving rise to chiral edge states [4]. A similar scenario occurs in two-dimensional topological insulators without external magnetic fields, i.e., no time-reversal symmetry (TRS) breaking. This mechanism is induced by the intrinsic spin-orbit interaction (SOI) [5–7] acting as an effective magnetic field $\vec{B}_{\text{eff}}(\vec{k})$, which couples to the electron spin. $\vec{B}_{\text{eff}}(\vec{k})$ is an odd function of $\vec{k}$ due to time reversal symmetry, thus, electrons moving in opposite directions along the edges have opposite spin polarizations. This is known as the quantum spin Hall effect (QSHE) [8–10], where the edge states are topologically protected from backscattering due to spin-momentum locking and TRS [6,11]. The topological protection results in a dissipationless transport even in the presence of nonmagnetic disorder [6]. In three dimensions (3D), topological insulators are insulating bulk materials but possess metallic edges states located at the surface. The first 3D topological insulator identified experimentally was $Bi_{1-x}Sb_x$ [12]. Afterwards, a multitude of 3D topological insulators were discovered, such as Bi_2Se_3, Bi_2Te_3 and Sb_2Te_3 [5,13,14]. As a characteristic feature, the band structure of these materials displays a topological surface state that has a dispersion linear in $\vec{k}$ near the Γ point [5].

The TRS in topological insulators can be broken either by using an external magnetic field or by doping the material with magnetic impurities, which can generate numerous interesting effects. One of the most remarkable is the quantum anomalous Hall effect (QAHE), whereby the measured conductance is quantized to integer multiples of e^2/h, the integer being the Chern number of the system [15]. This effect has great potential for future devices with low power consumption that rely exclusively on the electron spin [16–18]. Interestingly, the doping of $Bi(Sb)_2Te_3$ and $(Bi_{1-x}Sb_x)_2Te_3$ with high concentrations of Cr magnetic impurities allowed the experimental realization of the QAHE at low temperatures [19–21]. The observation of the QAHE is a signature of a gap opening at the Dirac point. However, this gap opening is still a controversial point, which generated several experimental investigations on magnetically doped topological insulators. Chen *et al.* [13] used angle-resolved photoemission (ARPES) and showed that in nonmagnetically doped Bi_2Se_3 no gap opening is observed, while the presence of Fe impurities breaking TRS leads to a gap opening at the Γ point, which was attributed to the presence of a ferromagnetic order of the magnetic impurities. Similar observations concerning the gap opening were made later in Refs. [22–25]. Nonetheless, the observations made in Ref. [22] have been attributed to an artifact resulting from the quantization of the bulk bands [26]. Similarly, the findings of Ref. [23] were explained to arise from inhomogeneities present in the samples [27]. Furthermore, other experimental works reported the absence of a gap. Using ARPES, Scholz *et al.* [28] showed that Fe impurities deposited on a Bi_2Se_3 surface at high or low temperatures do not lead to a gap opening at the Dirac point. In fact, the surface state remains robust even for high impurity coverage. Afterwards, other works [29,30] combining various experimental methods (ARPES or scanning tunneling microscopy) with *ab initio* calculations did not report a gap opening at the Dirac point.

The existence of long range ferromagnetic order and the absence of a gap opening can be reconciled when

*j.bouaziz@fz-juelich.de
†m.dos.santos.dias@fz-juelich.de
‡s.lounis@fz-juelich.de

impurity-induced in-gap states are present. Indeed, based on scanning tunneling spectroscopy (STS) measurements and a phenomenological model for the topological surface state, Sessi *et al.* [31] showed that in-gap states lead to a local filling of the band gap in the presence of ferromagnetic order. These in-gap states consist of sharp resonances in the density of states lying within the bulk band gap [32,33] and had been interpreted as local signatures of topology [34]. Interestingly, similar resonances were also observed from experiment and first-principles calculations for 3*d* impurities deposited on a Cu(111) surface [35,36]. The resonances were located at the bottom of the surface state with a broadening caused by the hybridization with the bulk bands. The presence of these peaks is explained by the nature of the impurity potential, and its strength, which can attract or repel electronic states of the host material.

In topological insulators, the in-gap states have been investigated with phenomenological models [32,37], which relate their creation to the presence of topological surface states. The latter are modeled using a Dirac-like Hamiltonian with a linear dispersion [37]:

$$\boldsymbol{H}_{\mathrm{D}} = \hbar\, v_{\mathrm{F}}\, (\vec{\boldsymbol{\sigma}} \times \vec{k})_z, \tag{1}$$

with v_{F} being the Fermi velocity and $\vec{k}$ the electron momentum. The magnetic impurities are modeled by a scattering potential $\boldsymbol{V}(\vec{r})$, which contains a nonmagnetic and a magnetic part: $\boldsymbol{V}(\vec{r}) = (U\,\boldsymbol{\sigma}_0 - J\,\vec{M}\cdot\vec{\boldsymbol{\sigma}})\,\delta(\vec{r}-\vec{r}_n)$, $\boldsymbol{\sigma}_0$ is the 2×2 identity matrix. The spatial dependence of the potential is approximated by a delta function and $\vec{r}_n$ is the position of the impurity. U represents the strength of the charge scattering, while J is the coupling constant between the spin of the surface electrons and the magnetic moment $\vec{M}$ of the impurity. In the presence of a weak charge scattering (i.e., $\frac{U}{JM} < 1$) and when considering $\vec{M} \parallel z$, the energy dispersion is gapped near the Dirac point [37,38]. However, magnetic impurities can induce a strong charge scattering, which leads to the creation of in-gap states filling locally the band gap. This phenomenological model seems to provide several possible outcomes susceptible to explain the experimental observations. Nonetheless, it does not have a full description of the electronic structure and misses the contribution of the bulk bands, which may play a crucial role in the formation of these in-gap states.

In this paper, we explore the impact of the bulk bands on the in-gap states present in magnetically doped topological insulators [31,39,40]. We performed first-principles calculations for 3*d* transition metal impurities embedded in the surfaces of Bi_2Te_3 and Bi_2Se_3, fixing $\vec{M} \parallel z$. Our calculations show that the band gap is locally filled by impurity resonances, as predicted in Refs. [31,32,37]. Comparing with calculations for 3*d* impurities embedded in the bulk of Bi_2Te_3 and Bi_2Se_3, we demonstrate that the hybridization of the impurity *d* states with the *sp* bulk bands is the driving mechanism behind the formation of these in-gap states. A simple model is used to analyze our results.

This paper is organized as follows. In Sec. II, we describe the first-principles approach and provide the technical details used in the calculations. We also consider a simple Anderson model, which will be employed to understand the emergence of in-gap states in magnetically doped topological insulators. Section III is dedicated to the study of the in-gap states from first principles by highlighting the importance of the contribution of bulk states. Furthermore, we show the results of the local density of states obtained within the Anderson model and explore the possibility of creating in-gap states from hybridization with the bulk or the topological surface state. Finally, in Sec. IV we summarize our results.

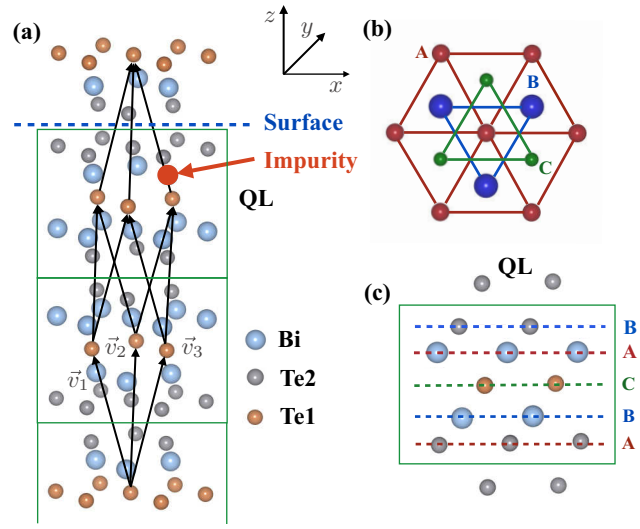

FIG. 1. Atomic structure. (a) Crystal structure of Bi_2Te_3 characterized by a primitive unit cell containing five inequivalent atoms (two Bi, two Te2, and one Te1). The rhombohedral primitive vectors $\{\vec{v}_1,\vec{v}_2,\vec{v}_3\}$ are also shown. For the slab, six quintuple layers are used. The cut to create the surface is indicated on the figure. The position of the impurity in the real space calculations is indicated by a red arrow. (b) Top view of the crystal structure showing the ABC stacking of the different layers. (c) Side view of the quintuple layer showing the stacking of the layers along the *z* direction.

II. DESCRIPTION OF THE METHODS AND COMPUTATIONAL ASPECTS

A. *Ab initio* method

Our first-principles simulations are performed using the Korringa-Kohn-Rostoker Green function (KKR-GF) method [41,42], which relies on multiple scattering theory. The calculations are carried out using the atomic sphere approximation (ASA) including full charge density in the local spin density approximation (LSDA), as parametrized by Vosko, Wilk, and Nusair [43]. We employ the scalar relativistic approach augmented self-consistently with SOI, which is of crucial importance in topological insulators. The calculations are made in two steps. First, we simulate the periodic host (bulk and surface), which is then used to self-consistently embed the impurities in real space.

The bulk unit cell includes five atoms and ten sites in total (i.e., five vacuum sites), see Fig. 1(a). The lattice parameters for the rhombohedral crystal structure are taken from experiment [44]. The system is self-consistently converged using $30\times 30\times 30$ *k* points in the full Brillouin zone. For the surface calculations, we used a slab containing six quintuple layers, which is enough to ensure the absence of a direct coupling

between the two surfaces, since the surface state penetrates only within two quintuple layers [44]. The slab was converged using a $60 \times 60 \times 1$ k mesh in the full Brillouin zone. Once the Green functions of the periodic system are obtained, the impurity is embedded self-consistently in a finite region in space (i.e., the perturbation in the potential due to the impurity has a finite range) using the following Dyson equation:

$$\begin{aligned} G_{\mathrm{I}}(\varepsilon) &= G_{\mathrm{H}}(\varepsilon) + G_{\mathrm{H}}(\varepsilon)\,(V_{\mathrm{I}} - V_{\mathrm{H}})\,G_{\mathrm{I}}(\varepsilon), \\ &= G_{\mathrm{H}}(\varepsilon) + G_{\mathrm{H}}(\varepsilon)\,\Delta V\,G_{\mathrm{I}}(\varepsilon), \end{aligned} \tag{2}$$

where the real space dependence is omitted for simplicity. V_{I} (V_{H}) is the Kohn-Sham potential in the cluster in the presence (absence) of the impurity. $G_{\mathrm{I}}(\varepsilon)$ represents the Green function of the system in the presence of the impurity, while $G_{\mathrm{H}}(\varepsilon)$ is the Green function of the undisturbed host. The $3d$ impurities are substituting a Bi atom from the subsurface layer as indicated in Fig. 1(a). This position is stable thermodynamically as observed experimentally and predicted from first principles for the case of Fe in Bi_2Te_3 [45,46]. We considered different real space cluster sizes and found that the quantities of interest (local density of states, spin, and orbital moments) are converged when considering a cluster containing 102 sites in total (24 Bi atoms, 31 Te (Se) atoms, and 47 vacuum sites).

B. Anderson model

In order to explain the origin of the in-gap states observed in the local density of states (LDOS) of the $3d$ impurities embedded in Bi_2Te_3 (Bi_2Se_3), we use a simple Anderson impurity model. Our goal is to understand if and how the hybridization with both bulk and surface states leads to the formation of in-gap states. We consider a minimal model to interpret our first-principles calculations, which takes into account an impurity with a single d orbital (as an example, we chose the d_{xy} component). The impurity has two energy levels $\varepsilon_i^{\uparrow}$ and $\varepsilon_i^{\downarrow}$ for the majority and minority spin channels, respectively. This impurity hybridizes with a two-dimensional topological insulator surface state, which is characterized by the linear Dirac Hamiltonian shown in Eq. (1). Furthermore, we account for the bulk bands by including Bloch states which are also characterized by the wave vector $\vec{k}$ and the eigenenergies $\varepsilon_{\vec{k}}^{\sigma}$ for each spin channel. The bulk and surface states interact only via the impurity. The impurity LDOS can be computed using the local Green function for which the spin diagonal part reads:

$$\boldsymbol{G}_i^{\sigma\sigma}(\varepsilon) = \frac{1}{\varepsilon - \varepsilon_i^{\sigma} - \Sigma(\varepsilon)}, \tag{3}$$

$\Sigma(\varepsilon)$ represents the hybridization function of the impurity. It describes the hybridization between the impurity d electrons and the host sp electrons. $\Sigma(\varepsilon) = \Lambda(\varepsilon) + \mathrm{i}\Delta(\varepsilon)$, with $\Lambda(\varepsilon)$ and $\Delta(\varepsilon)$ being the real and imaginary parts of $\Sigma(\varepsilon)$, respectively. For the purpose of our study, we consider the self-energy to be spin independent. The spin polarized LDOS of the impurity $n_i^{\sigma}(\varepsilon)$ is given by:

$$n_i^{\sigma}(\varepsilon) = -\frac{1}{\pi}\frac{\Delta(\varepsilon)}{(\varepsilon - \varepsilon_i^{\sigma} - \Lambda(\varepsilon))^2 + (\Delta(\varepsilon))^2}. \tag{4}$$

$\Sigma(\varepsilon)$ can also be decomposed into bulk and surface contributions:

$$\Sigma(\varepsilon) = \Sigma^{\mathrm{b}}(\varepsilon) + \Sigma^{\mathrm{s}}(\varepsilon), \tag{5}$$

where $\Sigma^{\mathrm{b}}(\varepsilon)$ and $\Sigma^{\mathrm{s}}(\varepsilon)$ represent the hybridization functions with the bulk and surface states, respectively. Moreover, we define $\Delta_{\mathrm{b}}(\varepsilon)$ ($\Delta_{\mathrm{s}}(\varepsilon)$) as the imaginary part of the bulk (surface) hybridization function, while $\Lambda_{\mathrm{b}}(\varepsilon)$ ($\Lambda_{\mathrm{s}}(\varepsilon)$) is the real part of the bulk (surface) hybridization function. Relying on Eq. (4), we expect in-gap states to occur when $\varepsilon - \varepsilon_i^{\sigma} - \Lambda_{\mathrm{b}}(\varepsilon) - \Lambda_{\mathrm{s}}(\varepsilon) \simeq 0$ and for $(\Delta_{\mathrm{b}}(\varepsilon) + \Delta_{\mathrm{s}}(\varepsilon))$ small. The LDOS of the impurities is mildly affected when they are moved from the surface to the bulk as shown in Fig. 2 and discussed in the next sections. Therefore, one can conclude that the coupling to the surface state is rather weak. $\Sigma_i^{\mathrm{b}}(\varepsilon)$ and $\Sigma_i^{\mathrm{s}}(\varepsilon)$ are derived analytically in Appendix A under the following assumptions: On one hand, the bulk band is modeled using a gapped density of states $n_{\mathrm{b}}(\varepsilon)$ given by:

$$n_{\mathrm{b}}(\varepsilon) = \begin{cases} n_{\mathrm{b}} & \text{for} \quad \varepsilon_{\mathrm{bv}} < \varepsilon < \varepsilon_{\mathrm{tv}}, \\ n_{\mathrm{b}} & \text{for} \quad \varepsilon_{\mathrm{bc}} < \varepsilon < \varepsilon_{\mathrm{tc}}, \\ 0 & \text{elsewhere.} \end{cases} \tag{6}$$

n_{b} is the occupation number in the valence and conduction band. $\varepsilon_{\mathrm{bv}}$ ($\varepsilon_{\mathrm{bc}}$) and $\varepsilon_{\mathrm{tv}}$ ($\varepsilon_{\mathrm{tc}}$) represent the bottom and the top of the valence (conduction) band, respectively. On the other hand, the surface state is described by the Dirac Hamiltonian given in Eq. (1). The LDOS of the surface states is linear within a certain energy window and is then connected to a flat LDOS, which is required to avoid spurious peaks in the LDOS at the cutoff energies $\pm\varepsilon_0$:

$$n_{\mathrm{s}}(\varepsilon) = \begin{cases} \frac{|\varepsilon - \varepsilon_{\mathrm{D}}|}{\varepsilon_0^2} & \text{for} \quad -\varepsilon_0 < \varepsilon < \varepsilon_0, \\ \frac{1}{\varepsilon_0} & \text{for} \quad \varepsilon_{\mathrm{tv}} < \varepsilon < -\varepsilon_0, \\ \frac{1}{\varepsilon_0} & \text{for} \quad \varepsilon_0 < \varepsilon < \varepsilon_{\mathrm{tc}}, \\ 0 & \text{elsewhere.} \end{cases} \tag{7}$$

ε_{D} being the energy of the Dirac point with respect to the Fermi energy (chosen to be the reference energy). This model can be parametrized using first-principles data, which we proceed to discuss next.

III. RESULTS AND DISCUSSION

A. In-gap states from first principles

We show in Table I the charge, spin, and orbital moments of single $3d$ transition metal impurities: Cr, Mn, Fe, and Co, which are embedded into the Bi_2Te_3 and Bi_2Se_3 surfaces. The spin moments are considered to be normal to each surface, since the out-of-plane orientation is a prerequisite for the potential gap opening [38]. The valence charge on the impurity is shown in the first column. We notice that all $3d$ impurities are donors of electrons (n-type doping). Similar results were obtained for Fe impurities in Bi_2Te_3 [45]. The second column in Table I displays the values of the spin moment M_{s}. Cr and Mn have a nearly half-filled d-shell and present high values for M_{s}, which decreases for Fe and Co following the Hund's rules. The values of the orbital moments (M_{l}) shown in the third column behave differently. High values are obtained for Fe and Co due to the partial filling of the minority d orbitals, in contrast to the low values of Cr and Mn. The impact of the

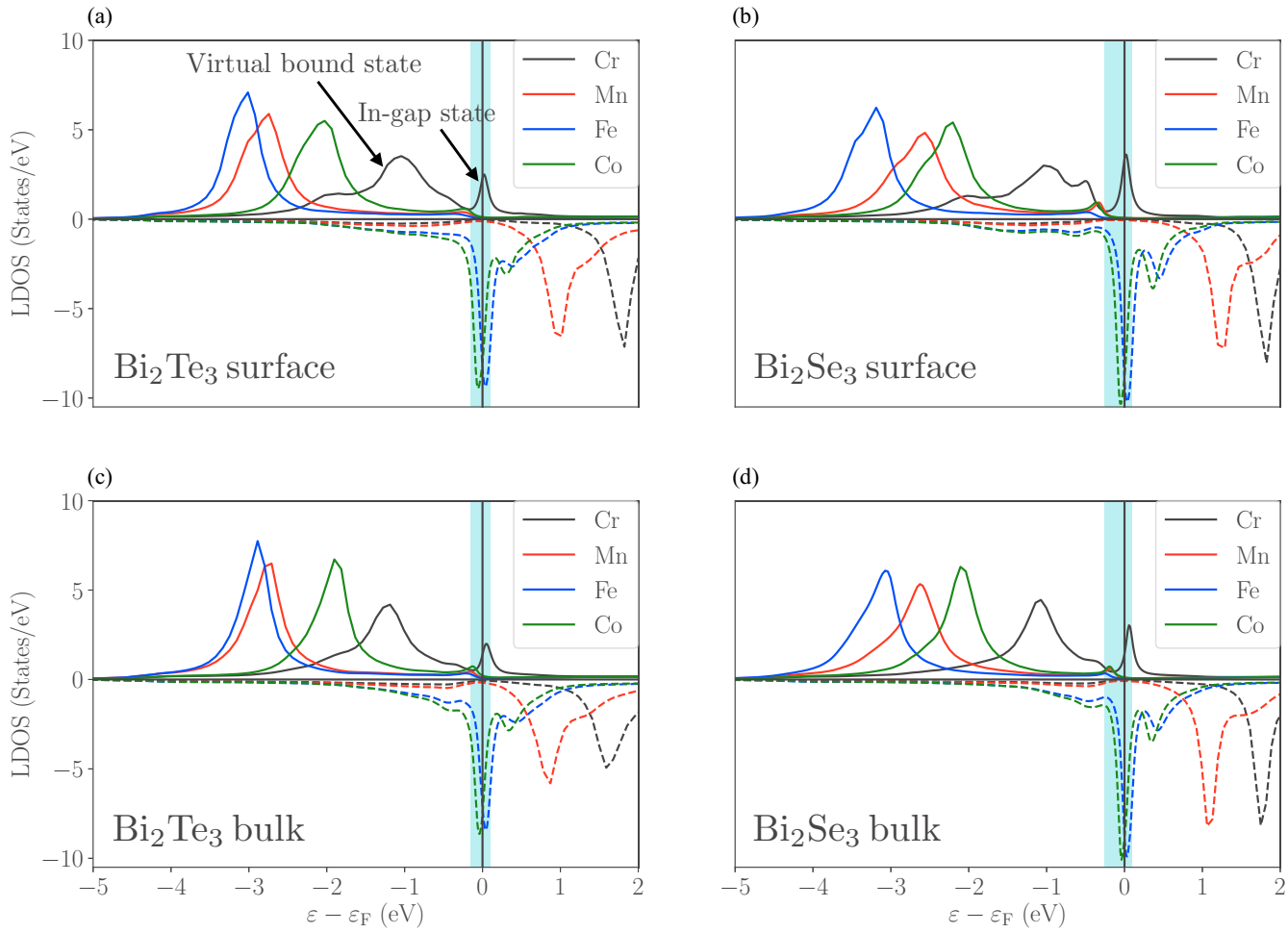

FIG. 2. First-principles simulated spin-resolved LDOS for 3*d* impurities (Cr, Mn, Fe, and Co) embedded in (a) the (111) surface of Bi_2Te_3, (b) the (111) surface of Bi_2Se_3, (c) the bulk of Bi_2Te_3, and (d) in the bulk of a Bi_2Se_3 bulk. The majority-spin channel is represented in full lines, while the minority-spin channel is given in dashed lines. The energies are given with respect to ε_F and the bulk band gap is highlighted in light blue.

chemical nature of the substrate was also investigated. When 3*d* impurities are embedded in the surface of Bi_2Se_3 instead of Bi_2Te_3, the following changes occur in the ground state quantities: First, the impurities tend to donate more electrons when embedded in Bi_2Se_3 than in Bi_2Te_3, which is in line with Se having a higher electronegativity than Te. Second, M_s decreases for Cr while it increases for Mn, Fe, and Co. Finally, M_l is substantially affected, largely decreasing in the case of Cr, Mn, and Fe, while increasing for Co (see Table I). This large effect of the substrate on the magnitude of M_l is due to the high sensitivity of this quantity to the details of the hybridization.

TABLE I. Ground state properties of 3*d* impurities embedded in the Bi_2Te_3 and Bi_2Se_3 (111) surfaces: valence charge on the impurity Q, spin moment M_s, and orbital moment M_l.

Element	Q	$M_s(\mu_B)$	$M_l(\mu_B)$
Cr (Bi_2Te_3)	5.154	3.843	0.065
Cr (Bi_2Se_3)	4.841	3.671	0.008
Mn (Bi_2Te_3)	6.160	4.412	0.050
Mn (Bi_2Se_3)	5.863	4.421	0.024
Fe (Bi_2Te_3)	7.282	3.395	0.260
Fe (Bi_2Se_3)	6.963	3.482	0.144
Co (Bi_2Te_3)	8.448	2.108	0.883
Co (Bi_2Se_3)	8.136	2.231	0.942

The LDOS of Cr, Mn, Fe, and Co embedded in the Bi_2Te_3 and Bi_2Se_3 surfaces are plotted in Figs. 2(a) and 2(b). The bulk band gap (light blue band in the figure) is ≈0.25 eV for Bi_2Te_3 and ≈0.35 eV for Bi_2Se_3 in agreement with the results of Ref. [5]. The majority spin channel (↑) is represented in full lines, while the minority spin channel (↓) is plotted with dashed lines. On one hand, the majority-spin channel is fully occupied for all considered elements with the exception of Cr. On the other hand, the minority-spin channel is partially occupied for Fe and Co and remains empty for Cr and Mn. The LDOS consists of a set of the so-called virtual bound states resulting from the hybridization of the atomic *d* orbitals of the impurity with the *sp* states of the Bi_2Te_3 host, resulting in a fractional valence charge of the impurity (see Table I). These resonances occur in both spin channels. Around ε_F, electronic states emerge in the bulk band gap of the substrate. These

are the in-gap states central to our study, which were already observed for Cr (Mn) doped Bi_2Se_3 (Bi_2Te_3) in Refs. [39,40].

From Fig. 2, we also notice that the presence of the in-gap states correlates with an impurity virtual bound state being close in energy to the bulk band gap ensuring the presence of electrons, which can be localized at the band edges (example: majority spin channel of Cr, Co). However, a d peak located too close to the bulk band edges might merge with the in-gap states (example: minority spin channel of Fe and Co in Bi_2Te_3). In this case, it is difficult to disentangle the in-gap state from the virtual bound state or one can even state that the latter becomes an in-gap state. For the investigated magnetic impurities, the in-gap state occurs only in one of the spin channels (either majority or minority spin), which leads to a large spin polarization at the Fermi energy. In other words, a local half-metallic behavior emerges from the in-gap states. Our simulations also suggest that in principle Cr impurities would lead to a clear experimental observation of in-gap states because they are well separated from the virtual bound states. Of course, such an observation using scanning tunneling spectroscopy would require us to consider the orbital nature of the in-gap state, which is dictated by the nature of the impurity.

The appearance of in-gap states near the bulk band edges suggests that they are connected. In order to remove the contribution of the surface state to the in-gap states, we computed the electronic structure of the $3d$ impurities embedded in bulk Bi_2Te_3 and Bi_2Se_3. Naturally, the impurities are substituting a Bi atom similarly to the surface case. The change in ground state properties (charge, spin, and orbital moments) of the impurities is rather small, and this can be understood from the fact that the immediate environment of the impurity (nearest neighbors) remains unchanged from surface to bulk. The LDOS is shown in Figs. 2(c) and 2(d), where we clearly observe that the in-gap state is still present for impurities in the bulk. Thus, we unambiguously prove that they originate from hybridization of the impurities d states with the host bulk band edges. In the next section, we will discuss the emergence of the in-gap states by means of a simple Anderson impurity model including contributions from a gapped bulk and a topological surface state.

B. In-gap states in the Anderson model

The results shown here are produced using the Anderson impurity model discussed in Sec. II B. We focus on the majority LDOS since it displays in-gap states which are not merged with the virtual bound states. Furthermore, a detailed analysis of the lm-resolved LDOS shows that the in-gap states are observed in the $\{d_{xy}, d_{x^2-y^2}, d_{xz}, d_{yz}\}$ partial contributions to the LDOS, but not in the d_{z^2} one. For clarity, we consider only the d_{xy} orbital. The model parameters are obtained as follows: First, we determine the center of the band $\varepsilon_i^{\uparrow}$ of d_{xy} component of the impurity LDOS. Then, the broadening of the states is assumed to be similar for all $3d$ impurities and is used to determine the strength of the coupling to the bulk $\langle V_{\vec{k}i}^{\mathrm{b}} \rangle$. The occupation of the host bulk LDOS $n_{\mathrm{b}}(\varepsilon)$ is also obtained from first principles. The energies corresponding to the bottom of the valence and the top of the conduction are cutoffs for numerical convenience (not realistic values). A similar procedure is employed to obtain the surface state parameters. Finally, we add an artificial broadening η to account for the small imaginary part of the energy present in our first-principles simulations. All the model parameters are listed in Table II.

TABLE II. Anderson model parameters used to compute the majority LDOS for the considered $3d$ impurities, the bulk hybridization function, and surface hybridization function. η is an artificial broadening added to mimic the small imaginary part of the energy included in our first-principles simulations. All the parameters are given in eV except n_{b} which is given in states/eV.

Bi_2Te_3 (bulk)	$\varepsilon_{\mathrm{bv}}$	$\varepsilon_{\mathrm{tv}}$	$\varepsilon_{\mathrm{bc}}$	$\varepsilon_{\mathrm{tc}}$	n_{b}	$\langle V_{\vec{k}i}^{\mathrm{b}} \rangle$
	−10.0	−0.1	0.1	10.0	0.15	1.15
Bi_2Te_3 (surface)	$\varepsilon_{\mathrm{bv}}$	$\varepsilon_{\mathrm{tc}}$	ε_0	ε_{D}	$\langle V_{\vec{k}i}^{s} \rangle$	
	−10.0	10.0	0.3	−0.2	0.25	
$3d$ elements	$\varepsilon_{\mathrm{Cr}}^{\uparrow}$	$\varepsilon_{\mathrm{Mn}}^{\uparrow}$	$\varepsilon_{\mathrm{Fe}}^{\uparrow}$	$\varepsilon_{\mathrm{Co}}^{\uparrow}$	η	
	−1.10	−2.70	−2.94	−1.98	0.02	

The components of the hybridization functions with the bulk and the surface state are shown in Fig. 3(b). $\Delta_{\mathrm{b}}(\varepsilon + i\eta)$ is a constant function in the valence and conduction bands, while it almost vanishes in the bulk band gap. $\Lambda_{\mathrm{b}}(\varepsilon + i\eta)$ represents the Hilbert transform of $\Delta_{\mathrm{b}}(\varepsilon + i\eta)$ and displays sharp features at the edges of the bulk band gap. $\Delta_{\mathrm{s}}(\varepsilon + i\eta)$ has a linear behavior for $\varepsilon \in [-0.5, 0.1]$ eV and is a constant otherwise. $\Lambda_{\mathrm{s}}(\varepsilon + i\eta)$ does not have any sharp feature. In Fig. 3(a), we show the model majority LDOS for our $3d$ impurities embedded in Bi_2Te_3 bulk. The in-gap states observed at the bulk band edges emerge due to high values in $\Lambda_{\mathrm{b}}(\varepsilon + i\eta)$ combined with small values for $\Delta_{\mathrm{b}}(\varepsilon + i\eta)$ (gap region). The model reproduces qualitatively the position and shape of the in-gap states for Mn, Fe, and Co. Furthermore, we obtain a clear feature in the LDOS of Cr. However, it is located at the lower bulk band edge in contrast to what is observed from first principles as shown in Fig. 2(c).

Considering only the topological surface state in Eq. (4), the condition to observe an in-gap state is: $\varepsilon - \varepsilon_i^{\uparrow} \simeq \Lambda_{\mathrm{s}}(\varepsilon)$ and $\Delta_{\mathrm{s}}(\varepsilon)$ must be small in order to increase the spectral weight. In other words, $\Lambda_{\mathrm{s}}(\varepsilon)$ and $\varepsilon - \varepsilon_i^{\uparrow}$ must ideally cross each other in a region where the substrate LDOS is low, i.e., close to the Dirac point (near ε_{D}). As an example, we take $\langle V_{\vec{k}i}^{s} \rangle = 0.25$ eV (smaller compared to the bulk one, see Table II) and plot in Fig. 3 the real and imaginary parts of $\Sigma_i^{\mathrm{s}}(\varepsilon)$ and $\varepsilon - \varepsilon_i^{\uparrow}$ for the considered $3d$ impurities. The crossing near ε_{D} leading to an in-gap state is not observed for this particular case. Although it may occur for stronger couplings to the surface, this would be in contradiction with our first-principles calculations predicting a weak coupling to the surface state.

IV. CONCLUSIONS

In this paper, we combined a first-principles and model approach to understand the emergence and origins of in-gap states in the LDOS of $3d$ transition metal impurities embedded in topologically insulating hosts, which consist of Bi_2Te_3 and Bi_2Se_3. We considered bulk systems and thin films. We found that ground state properties such as the valence charge, spin, and orbital moment on the impurity can be affected when trading the Bi_2Te_3 host for the Bi_2Se_3 one. The largest changes were noticed for the orbital moments. Our first-principles

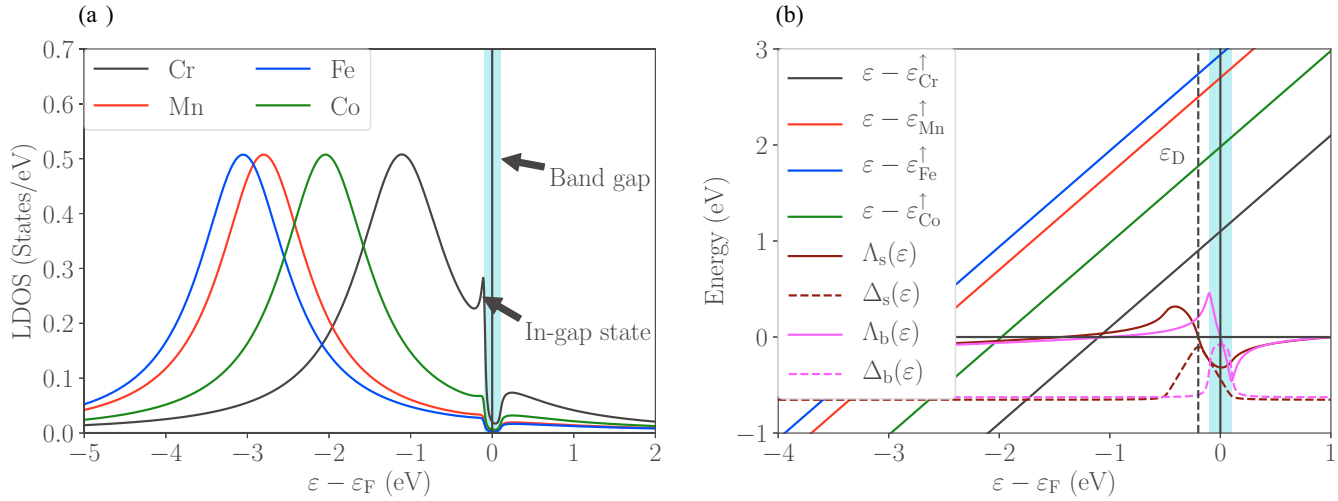

FIG. 3. (a) Modeled d_{xy} contribution to the majority LDOS of Cr, Mn, Fe, and Co embedded in Bi_2Te_3 bulk within the Anderson model. (b) The straight lines represent $\varepsilon - \varepsilon_i^{\uparrow}$, where $\varepsilon_i^{\uparrow}$ is the energy level of the majority d_{xy} orbital. The real and imaginary parts of the bulk (surface) hybridization function are depicted in magenta (brown). The Dirac point is located at $\varepsilon_D = -0.2$ eV. The used model parameters are given in Table II.

simulations showed the emergence of in-gap states when the impurities are embedded in the bulk, ruling out the necessity of the topological surface state for their creation. Furthermore, we built an Anderson model where the impurity contains a single d orbital which hybridizes with bulk and surface states. Within this model, we showed that the in-gap states arise at the bulk band edges from the real part of the bulk hybridization function. We also considered the possibility of creating in-gap states when considering solely the topological surface state. However, this requires large and nonphysical coupling constants between the $3d$ impurities and the topological surface states.

For the investigated systems, the in-gap states are found in one single spin channel, which generates a half-metallic behavior at the impurity site and its immediate surrounding. Also the orbital nature of these localized states depend on the electronic filling of the impurity.

Our results are in good agreement with the STS measurements obtained in Refs. [29,31], which display a finite local density of states within the gap region when the tip is located above the defects ($3d$ impurities). This finite density of states is attributed to the presence of in-gap states leading to a filling of the band gap locally. Furthermore, the in-gap states reported in this paper were also observed previously from first-principles calculations for Cr (Mn) in $Bi_2Se(Te)_3$ in Refs. [39,40] but without relating their existence to the hybridization with the bulk bands. Our calculations demonstrate the insufficiency of the most commonly adopted models [32,37], which focus exclusively on the Dirac-like surface state. With suitable extensions, the in-gap states can also be recovered in the bulk at the model level [33,37], as we also showed relying on our simplified Anderson model. We point out that the impurity-induced in-gap states are strongly localized in the vicinity of the impurities, so that at larger distances the magnetic proximity effect could still lead to a gap in density of states (of the surface state). This could support a quantum anomalous Hall state [31,47,48].

Finally, the in-gap states provide a relatively high density of states at the Fermi energy which may profoundly alter the magnetic properties of the system, for instance: the magnetic anisotropy energy [49,50], the response of the impurities to external time-dependent perturbations [51–53], their magnetic stability against spin fluctuations [54], and many other phenomena. These properties are currently under investigation.

ACKNOWLEDGMENTS

We thank P. Rüssmann for fruitful discussions and for providing the potentials and initial setups for the topological insulating host (Bi_2Te_3). This work was supported by the European Research Council (ERC) under the European Union's Horizon 2020 research and innovation programme (ERC-consolidator Grant No. 681405 DYNASORE). We gratefully acknowledge the computing time granted by the JARA-HPC Vergabegremium and VSR commission on the supercomputer JURECA at Forschungszentrum Jülich.

APPENDIX: BULK AND SURFACE HYBRIDIZATION FUNCTION FOR THE ANDERSON MODEL

Here, we analytically derive the real and imaginary parts of $\Sigma_i^b(\varepsilon)$ and $\Sigma_i^b(\varepsilon)$. We assume that $V_{\vec{k}i}^b$ is weakly depending on $\vec{k}$:

$$\begin{aligned}\Sigma_i^b(\varepsilon + i\eta) &= \sum_{\vec{k}} \frac{|V_{\vec{k}i}^b|^2}{\varepsilon - \varepsilon_{\vec{k}} + i\eta}, \\ &= |\langle V_{\vec{k}i}^b \rangle|^2 \sum_{\vec{k}} \frac{1}{\varepsilon - \varepsilon_{\vec{k}} + i\eta}, \\ &= |\langle V_{\vec{k}i}^b \rangle|^2 \int d\varepsilon' \frac{n_b(\varepsilon')}{\varepsilon - \varepsilon' + i\eta}. \end{aligned} \tag{A1}$$

Using the definition of $n_b(\varepsilon)$ given in Eq. (6), $\Lambda_b(\varepsilon + i\eta)$ reads:

$$\Lambda_b(\varepsilon + i\eta) = -\frac{n_b\left|\langle V_{\vec{k}i}^b\rangle\right|^2}{2}\left[\ln\left(\frac{(\varepsilon-\varepsilon_{tv})^2+\eta^2}{(\varepsilon-\varepsilon_{bv})^2+\eta^2}\right)+\ln\left(\frac{(\varepsilon-\varepsilon_{tc})^2+\eta^2}{(\varepsilon-\varepsilon_{bc})^2+\eta^2}\right)\right], \tag{A2}$$

and the imaginary part is:

$$\begin{aligned}\Delta_b(\varepsilon + i\eta) = {} & n_b\left|\langle V_{\vec{k}i}^b\rangle\right|^2\left[\arctan\left(\frac{\varepsilon-\varepsilon_{tv}}{\eta}\right)-\arctan\left(\frac{\varepsilon-\varepsilon_{bv}}{\eta}\right)\right] \\ & + n_b|\langle V_{\vec{k}i}^b\rangle|^2\left[\arctan\left(\frac{\varepsilon-\varepsilon_{tc}}{\eta}\right)-\arctan\left(\frac{\varepsilon-\varepsilon_{bc}}{\eta}\right)\right].\end{aligned} \tag{A3}$$

Once more, assuming that $V_{\vec{k}i}^s$ depends weakly on $\vec{k}$, the real part of $\Sigma_i^s(\varepsilon)$ reads:

$$\begin{aligned}\Lambda_s(\varepsilon + i\eta) = {} & \frac{\left|\langle V_{\vec{k}i}^s\rangle\right|^2\varepsilon}{2\varepsilon_0^2}\left[\ln\left(\frac{\varepsilon_r^2+\eta^2}{(\varepsilon_r+\varepsilon_0)^2+\eta^2}\right)-\ln\left(\frac{(\varepsilon_r-\varepsilon_0)^2+\eta^2}{\varepsilon_r^2+\eta^2}\right)\right] \\ & + \frac{\left|\langle V_{\vec{k}i}^s\rangle\right|^2\eta}{\varepsilon_0^2}\left[2\arctan\left(\frac{\varepsilon_r}{\eta}\right)-\arctan\left(\frac{\varepsilon_r+\varepsilon_0}{\eta}\right)-\arctan\left(\frac{\varepsilon_r-\varepsilon_0}{\eta}\right)\right] \\ & - \frac{\left|\langle V_{\vec{k}i}^s\rangle\right|^2}{2\varepsilon_0}\left[\ln\left(\frac{(\varepsilon_r+\varepsilon_0)^2+\eta^2}{(\varepsilon_r-\varepsilon_{bv})^2+\eta^2}\right)+\ln\left(\frac{(\varepsilon_r-\varepsilon_{tc})^2+\eta^2}{(\varepsilon_r-\varepsilon_0)^2+\eta^2}\right)\right]\end{aligned} \tag{A4}$$

while the imaginary part reads:

$$\begin{aligned}\Delta_s(\varepsilon + i\eta) = {} & \frac{\left|\langle V_{\vec{k}i}^s\rangle\right|^2\eta}{2\varepsilon_0^2}\left[\ln\left(\frac{\varepsilon_r^2+\eta^2}{(\varepsilon_r+\varepsilon_0)^2+\eta^2}\right)-\ln\left(\frac{(\varepsilon_r-\varepsilon_0)^2+\eta^2}{\varepsilon_r^2+\eta^2}\right)\right] \\ & + \frac{\left|\langle V_{\vec{k}i}^s\rangle\right|^2\varepsilon_r}{\varepsilon_0^2}\left[2\arctan\left(\frac{\varepsilon_r}{\eta}\right)-\arctan\left(\frac{\varepsilon_r+\varepsilon_0}{\eta}\right)-\arctan\left(\frac{\varepsilon_r-\varepsilon_0}{\eta}\right)\right] \\ & + \frac{\left|\langle V_{\vec{k}i}^s\rangle\right|^2}{\varepsilon_0}\left[\arctan\left(\frac{\varepsilon_r+\varepsilon_0}{\eta}\right)-\arctan\left(\frac{\varepsilon_r-\varepsilon_{bv}}{\eta}\right)\right] \\ & + \frac{\left|\langle V_{\vec{k}i}^s\rangle\right|^2}{\varepsilon_0}\left[\arctan\left(\frac{\varepsilon_r-\varepsilon_{tc}}{\eta}\right)-\arctan\left(\frac{\varepsilon_r-\varepsilon_0}{\eta}\right)\right],\end{aligned} \tag{A5}$$

with $\varepsilon_r = \varepsilon - \varepsilon_D$.

[1] K. v. Klitzing, G. Dorda, and M. Pepper, New Method for High-Accuracy Determination of the Fine-Structure Constant Based on Quantized Hall Resistance, Phys. Rev. Lett. **45**, 494 (1980).

[2] K. von Klitzing, The quantized Hall effect, Rev. Mod. Phys. **58**, 519 (1986).

[3] E. H. Hall, On a new action of the magnet on electric currents, American Journal of Mathematics **2**, 287 (1879).

[4] B. I. Halperin, Quantized hall conductance, current-carrying edge states, and the existence of extended states in a two-dimensional disordered potential, Phys. Rev. B **25**, 2185 (1982).

[5] H. Zhang, C. X. Liu, X. L. Qi, X. Dai, Z. Fang, and S. C. Zhang, Topological insulators in Bi_2Te_3, Bi_2Se_3 and Sb_2Te_3 with a single Dirac cone on the surface, Nat. Phys. **5**, 438 (2009).

[6] M. Z. Hasan and C. L. Kane, Colloquium: Topological insulators, Rev. Mod. Phys. **82**, 3045 (2010).

[7] X.-L. Qi and S.-C. Zhang, Topological insulators and superconductors, Rev. Mod. Phys. **83**, 1057 (2011).

[8] C. L. Kane and E. J. Mele, Quantum Spin Hall Effect in Graphene, Phys. Rev. Lett. **95**, 226801 (2005).

[9] L. Fu and C. L. Kane, Topological insulators with inversion symmetry, Phys. Rev. B **76**, 045302 (2007).

[10] M. König, S. Wiedmann, C. Brüne, A. Roth, H. Buhmann, L. W. Molenkamp, X. L. Qi, and S. C. Zhang, Quantum spin Hall insulator state in HgTe quantum wells, Science **318**, 766 (2007).

[11] L. Fu, C. L. Kane, and E. J. Mele, Topological Insulators in three Dimensions, Phys. Rev. Lett. **98**, 106803 (2007).

[12] D. Hsieh, D. Qian, L. Wray, Y. Q. Xia, Y. S. Hor, R. J. Cava, and M. Z. Hasan, A topological Dirac insulator in a quantum spin Hall phase (experimental realization of a 3D topological insulator), Nature (London) **452**, 970 (2008).

[13] Y. L. Chen, J. H. Chu, J. G. Analytis, Z. K. Liu, K. Igarashi, H. H. Kuo, X. L. Qi, S. K. Mo, R. G. Moore, D. H. Lu, M. Hashimoto, T. Sasagawa, S. C. Zhang, I. R. Fisher, Z. Hussain, and Z. X. Shen, Massive Dirac Fermion on the surface of a magnetically doped topological insulator, Science **329**, 659 (2010).

[14] Y. S. Hor, A. Richardella, P. Roushan, Y. Xia, J. G. Checkelsky, A. Yazdani, M. Z. Hasan, N. P. Ong, and R. J. Cava, p-type Bi_2Te_3 for topological insulator and low-temperature thermoelectric applications, Phys. Rev. B **79**, 195208 (2009).

[15] C.-X. Liu, S.-C. Zhang, and X.-L. Qi, The quantum anomalous hall effect: Theory and experiment, Annu. Rev. Condens. Matter Phys. **7**, 301 (2016).

[16] I. Garate and M. Franz, Inverse Spin-Galvanic Effect in the Interface Between a Topological Insulator and a Ferromagnet, Phys. Rev. Lett. **104**, 146802 (2010).

[17] L. Fu and C. L. Kane, Probing Neutral Majorana Fermion Edge Modes with Charge Transport, Phys. Rev. Lett. **102**, 216403 (2009).

[18] W. K. Tse and A. H. MacDonald, Giant Magneto-Optical Kerr Effect and Universal Faraday Effect in Thin-Film Topological Insulators, Phys. Rev. Lett. **105**, 057401 (2010).

[19] C. Z. Chang, J. Zhang, X. Feng, J. Shen, Z. Zhang, M. Guo, K. Li, Y. Ou, P. Wei, L. L. Wang, Z. Q. Ji, Y. Feng, S. Ji, X. Chen, J. Jia, X. Dai, Z. Fang, S. C. Zhang, K. He, Y. Wang, L. Lu, X. C. Ma, and Q. Xue, Experimental observation of the quantum anomalous Hall effect in a magnetic topological insulator, Science **340**, 167 (2013).

[20] X. Kou, S.-T. Guo, Y. Fan, L. Pan, M. Lang, Y. Jiang, Q. Shao, T. Nie, K. Murata, J. Tang, Y. Wang, L. He, T.-K. Lee, W.-L. Lee, and K. L. Wang, Scale-Invariant Quantum Anomalous Hall Effect in Magnetic Topological Insulators Beyond the Two-Dimensional Limit, Phys. Rev. Lett. **113**, 137201 (2014).

[21] J. G. Checkelsky, R. Yoshimi, A. Tsukazaki, K. S. Takahashi, Y. Kozuka, J. Falson, M. Kawasaki, and Y. Tokura, Trajectory of the anomalous hall effect towards the quantized state in a ferromagnetic topological insulator, Nat. Phys. **10**, 731 (2014).

[22] L. A. Wray, S. Y. Xu, Y. Xia, D. Hsieh, A. V. Fedorov, Y. S. Hor, R. J. Cava, A. Bansil, H. Lin, and M. Z. Hasan, A topological insulator surface under strong Coulomb, magnetic and disorder perturbations, Nat. Phys. **7**, 32 (2011).

[23] S. Y. Xu, M. Neupane, C. Liu, D. Zhang, A. Richardella, L. A. Wray, N. Alidoust, M. Leandersson, T. Balasubramanian, J. Sánchez-Barriga, O. Rader, G. Landolt, B. Slomski, J. Hugo Dil, J. Osterwalder, T. R. Chang, H. T. Jeng, H. Lin, A. Bansil, N. Samarth, and M. Z. Hasan, Hedgehog spin texture and Berry's phase tuning in a magnetic topological insulator, Nat. Phys. **8**, 616 (2012).

[24] I. Lee, C. K. Kim, J. Lee, S. J. L. Billinge, R. Zhong, J. A. Schneeloch, T. Liu, T. Valla, J. M. Tranquada, G. Gu, and J. C. S. Davis, Imaging Dirac-mass disorder from magnetic dopant atoms in the ferromagnetic topological insulator $Cr_x(Bi_{0.1}Sb_{0.9})_{2-x}Te_3$, Proc. Natl. Acad. Sci. U.S.A. **112**, 1316 (2015).

[25] J. Sánchez-Barriga, A. Varykhalov, G. Springholz, H. Steiner, R. Kirchschlager, G. Bauer, O. Caha, E. Schierle, E. Weschke, A. A. Ünal *et al.*, Nonmagnetic band gap at the Dirac point of the magnetic topological insulator $(Bi_{1-x}Mn_x)_2Se_3$, Nat. Commun. **7**, 10559 (2016).

[26] M. Bianchi, R. C. Hatch, J. Mi, B. B. Iversen, and P. Hofmann, Simultaneous Quantization of Bulk Conduction and Valence States through Adsorption of Nonmagnetic Impurities on bi_2se_3, Phys. Rev. Lett. **107**, 086802 (2011).

[27] D. Zhang, A. Richardella, D. W. Rench, S.-Y. Xu, A. Kandala, T. C. Flanagan, H. Beidenkopf, A. L. Yeats, B. B. Buckley, P. V. Klimov, D. D. Awschalom, A. Yazdani, P. Schiffer, M. Z. Hasan, and N. Samarth, Interplay between ferromagnetism, surface states, and quantum corrections in a magnetically doped topological insulator, Phys. Rev. B **86**, 205127 (2012).

[28] M. R. Scholz, J. Sánchez-Barriga, D. Marchenko, A. Varykhalov, A. Volykhov, L. V. Yashina, and O. Rader, Tolerance of Topological Surface States Towards Magnetic Moments: Fe on Bi_2Se_3, Phys. Rev. Lett. **108**, 256810 (2012).

[29] J. Honolka, A. A. Khajetoorians, V. Sessi, T. O. Wehling, S. Stepanow, J. L. Mi, B. B. Iversen, T. Schlenk, J. Wiebe, N. B. Brookes, A. I. Lichtenstein, Ph. Hofmann, K. Kern, and R. Wiesendanger, In-plane Magnetic Anisotropy of Fe Atoms on Bi_2Se_3(111), Phys. Rev. Lett. **108**, 256811 (2012).

[30] T. Schlenk, M. Bianchi, M. Koleini, A. Eich, O. Pietzsch, T. O. Wehling, T. Frauenheim, A. Balatsky, J. L. Mi, B. B. Iversen, J. Wiebe, A. A. Khajetoorians, Ph. Hofmann, and R. Wiesendanger, Controllable Magnetic Doping of the Surface State of a Topological Insulator, Phys. Rev. Lett. **110**, 126804 (2013).

[31] P. Sessi, R. R. Biswas, T. Bathon, O. Storz, S. Wilfert, A. Barla, K. A. Kokh, O. E. Tereshchenko, K. Fauth, M. Bode *et al.*, Dual nature of magnetic dopants and competing trends in topological insulators, Nat. Commun. **7**, 12027 (2016).

[32] R. R. Biswas and A. V. Balatsky, Impurity-induced states on the surface of three-dimensional topological insulators, Phys. Rev. B **81**, 233405 (2010).

[33] A. M. Black-Schaffer and A. V. Balatsky, Subsurface impurities and vacancies in a three-dimensional topological insulator, Phys. Rev. B **86**, 115433 (2012).

[34] R.-J. Slager, L. Rademaker, J. Zaanen, and L. Balents, Impurity-bound states and green's function zeros as local signatures of topology, Phys. Rev. B **92**, 085126 (2015).

[35] L. Limot, E. Pehlke, J. Kröger, and R. Berndt, Surface-State Localization at Adatoms, Phys. Rev. Lett. **94**, 036805 (2005).

[36] S. Lounis, P. Mavropoulos, P. H. Dederichs, and S. Blügel, Surface-state scattering by adatoms on noble metals: Ab initio calculations using the Korringa-Kohn-Rostoker Green function method, Phys. Rev. B **73**, 195421 (2006).

[37] A. M. Black-Schaffer, A. V. Balatsky, and J. Fransson, Filling of magnetic-impurity-induced gap in topological insulators by potential scattering, Phys. Rev. B **91**, 201411 (2015).

[38] Q. Liu, C. X. Liu, C. Xu, X. L. Qi, and S. C. Zhang, Magnetic Impurities on the Surface of a Topological Insulator, Phys. Rev. Lett. **102**, 156603 (2009).

[39] L. Chotorlishvili, A. Ernst, V. K. Dugaev, A. Komnik, M. G. Vergniory, E. V. Chulkov, and J. Berakdar, Magnetic fluctuations in topological insulators with ordered magnetic adatoms: Cr on bi_2se_3 from first principles, Phys. Rev. B **89**, 075103 (2014).

[40] V. N. Antonov, L. V. Bekenov, S. Uba, and A. Ernst, Electronic structure and x-ray magnetic circular dichroism in mn-doped topological insulators bi_2se_3 and bi_2te_3, Phys. Rev. B **96**, 224434 (2017).

[41] D. S. G. Bauer, *Development of a Relativistic Full-Potential First-Principles Multiple Scattering Green Function Method Applied to Complex Magnetic Textures of Nano Structures at Surfaces* (Forschungszentrum Jülich, Jülich, 2013), Vol. 79, p. 193 S.

[42] N. Papanikolaou, R. Zeller, and P. H. Dederichs, Conceptual improvements of the kkr method, J. Phys.: Condens. Matter **14**, 2799 (2002).

[43] S. H. Vosko, L. Wilk, and M. Nusair, Accurate spin-dependent electron liquid correlation energies for local spin density

calculations: a critical analysis, Can. J. Phys. **58**, 1200 (1980).

[44] W. Zhang, R. Yu, H.-J. Zhang, X. Dai, and Z. Fang, First-principles studies of the three-dimensional strong topological insulators Bi_2Te_3, Bi_2Se_3 and Sb_2Te_3, New J. Phys. **12**, 065013 (2010).

[45] D. West, Y. Y. Sun, S. B. Zhang, T. Zhang, X. Ma, P. Cheng, Y. Y. Zhang, X. Chen, J. F. Jia, and Q. K. Xue, Identification of magnetic dopants on the surfaces of topological insulators: Experiment and theory for Fe on Bi_2Se_3(111), Phys. Rev. B **85**, 081305 (2012).

[46] L. B. Abdalla, L. Seixas, T. M. Schmidt, R. H. Miwa, and A. Fazzio, Topological insulator Bi_2Se_3(111) surface doped with transition metals: An ab initio investigation, Phys. Rev. B **88**, 045312 (2013).

[47] M. F. Islam, C. M. Canali, A. Pertsova, A. Balatsky, S. K. Mahatha, C. Carbone, A. Barla, K. A. Kokh, O. E. Tereshchenko, E. Jiménez, N. B. Brookes, P. Gargiani, M. Valvidares, S. Schatz, T. R. F. Peixoto, H. Bentmann, F. Reinert, J. Jung, T. Bathon, K. Fauth, M. Bode, and P. Sessi, Systematics of electronic and magnetic properties in the transition metal doped sb_2te_3 quantum anomalous hall platform, Phys. Rev. B **97**, 155429 (2018).

[48] T. R. F. Peixoto, H. Bentmann, S. Schreyeck, M. Winnerlein, C. Seibel, H. Maaß, M. Al-Baidhani, K. Treiber, S. Schatz, S. Grauer, C. Gould, K. Brunner, A. Ernst, L. W. Molenkamp, and F. Reinert, Impurity states in the magnetic topological insulator V : $(Bi,Sb)_2te_3$, Phys. Rev. B **94**, 195140 (2016).

[49] Š. Pick, V. S. Stepanyuk, A. N. Baranov, W. Hergert, and P. Bruno, Effect of atomic relaxations on magnetic properties of adatoms and small clusters, Phys. Rev. B **68**, 104410 (2003).

[50] D.-S. Wang, R. Wu, and A. J. Freeman, First-principles theory of surface magnetocrystalline anisotropy and the diatomic-pair model, Phys. Rev. B **47**, 14932 (1993).

[51] S. Lounis, A. T. Costa, R. B. Muniz, and D. L. Mills, Dynamical Magnetic Excitations of Nanostructures from first Principles, Phys. Rev. Lett. **105**, 187205 (2010).

[52] M. dos Santos Dias, B. Schweflinghaus, S. Blügel, and S. Lounis, Relativistic dynamical spin excitations of magnetic adatoms, Phys. Rev. B **91**, 075405 (2015).

[53] S. Lounis, M. dos Santos Dias, and B. Schweflinghaus, Transverse dynamical magnetic susceptibilities from regular static density functional theory: Evaluation of damping and g shifts of spin excitations, Phys. Rev. B **91**, 104420 (2015).

[54] J. Ibañez-Azpiroz, M. dos Santos Dias, S. Blügel, and S. Lounis, Zero-point spin-fluctuations of single adatoms, Nano Lett. **16**, 4305 (2016).